

DEPARTMENT OF ELECTRICAL AND
COMPUTER ENGINEERING

SCHOOL OF ENGINEERING
UNIVERSITY OF NEW MEXICO

ITERATIVE LEARNING CONTROL APPLICATIONS TO
HIGH POWER MICROWAVE TUBES

V. S. Soualian, G.T. Park, C.T. Abdallah, and E. Schamiloglu
EECE Department,
University of New Mexico,
Albuquerque, NM 87131, USA.

UNM Technical Report: EECE98-005

Report Date: July 21, 1998

Abstract

In this paper, we present a “smart” high-peak power microwave tube, by implementing iterative learning control methodologies to control a repetitively-pulsed, high-power, backward wave oscillator. The learning control algorithm is used to drive the error between the actual output and its desired value to zero. The desired output may be a given power level, a given frequency, or a combination of both. The learning control methodology is then verified in simulation and in hardware.

Acknowledgments

The work of all authors was supported through a High Energy Microwave Devices Consortium funded by an AFOSR/DOD MURI grant and administered through Texas Tech University.

1 Introduction

Present day high-peak power microwave (HPM) sources typically operate in the single shot regime because of practical limitations imposed by the pulsed power systems used to drive them [1, 2]. There are however commercial HPM systems that operate at modest repetition rates, two examples of which include a system based on the relatron source [3] operating at 1 Hz, and a system based on a magnetron source [4] operating at a 10 pulse per second burst mode. It is clear that a modest pulse repetition rate is attractive for practical implementation of an HPM system.

The physics of the interaction between a relativistic electron beam and various slow wave structure configurations in a short pulse backward-wave oscillator (BWO) has been studied experimentally and computationally in a collaborative effort between the University of New Mexico (USA) and the Institute of High Current Electronics (Tomsk, Russia) [5, 6]. The electron beam accelerator used in those studies is a Sinus-6 device that produces a 10 ns FWHM beam current pulsewidth, and can operate at a pulse repetition rate as large as 200 Hz. In practice, the accelerator operates at a pulse repetition rate no greater than 0.1 Hz, limited by the capacitor bank used to energize the magnetic field-producing solenoidal coil. A novel result of this effort was a demonstration of enhanced frequency agility of a high power BWO for constant electron beam and applied magnetic field parameters [6]. This agility was obtained through an axial displacement of the slow wave structure with respect to the “cutoff neck” inlet to the electrodynamic system. Furthermore, a companion study to this work provided a static, affine model of the input/output characteristics of the Sinus-6-driven BWO, and described how this information can be used as part of an algorithm to meet specific control objectives, such as maximizing the radiated frequency bandwidth for a fixed peak radiated microwave power level [7]. This was further expanded by automating the controller and verified via simulation in [8]. The next step in the research is then to implement the control algorithms on a physical tube in order to build a “smart tube” HPM source. By *smart tube* we mean an HPM source capable of adjusting its output characteristics to achieve certain preset criteria without operator intervention. Furthermore, a *smart tube* HPM source will *learn* from its earlier operation to affect its future performance. We believe that a *smart tube* HPM source represents an important development and will further the embodiment of these research devices into practical systems.

From a controls perspective, it turns out that the fast dynamics and changes in the operating characteristics of the BWO render traditional automatic control methods ineffective. In fact, our results in [7] for the Sinus-6-driven BWO have shown that a static, affine model is an accurate representation of its input/output characteristics. A static model is too fast to be controlled in real time while maintaining the same order dynamics (and thus the same bandwidth and speed of response) of the open-loop system. However, since the BWO we are studying is repetitively-pulsed, one can attempt to achieve the control objectives between pulses. More specifically, for control design purpose, an engineer is usually provided with a mathematical model of a *dynamical* system that can be described by differential/difference equations. The design problem is then reduced to finding a suitable control law to achieve some desired response. Research in controls has focused on the control of dynamical systems, since most physical systems exhibit some kind of dynamic behavior. Although a quantitative model may be difficult to obtain, once such a model is made available, the design part is relatively well-developed. On the other hand, the control problem for static systems is relatively undeveloped. Control issues for static systems have recently arisen in many areas such as rapid thermal processing [9], or in pulsed power systems [7]. Static systems may in fact have dynamics, but their input-output response is so fast, that they defy the usual description with differential/difference equations. One then has no hope of controlling such systems using standard control methodologies, unless their maneuvers are repeated over and over. Moreover, standard control issues such as stability may not arise when dealing with static systems, but others such as improving performance, optimality, and disturbance rejection will.

In this paper, we use an *iterative learning control* methodology on the static model of the repetitively-pulsed, Sinus-6 BWO. Given a mathematical model of the Sinus-6-driven BWO, one can solve for the desired input, given a desired output, by finding the inverse system. This open-loop control strategy works well if the system model is exact, is invertible, when no disturbances are present, and no issues of stability are involved. In practice however, the model is obtained from a set of noisy input-output data points, and an open-loop

control strategy is not sufficient. In addition, the BWO characteristics may be slowly varying due to changes in its operating conditions (jitter). In such a case, one has to account for any perturbations in the model and design a controller that takes them into account in generating the control law. Since as discussed above, the BWO system is extremely fast, we are not able to generate a control signal in real time while maintaining the speed of the response, and it is therefore logical to apply any control effort adjustments off-line, or in between successive shots [10]. One way to design such an off-line controller is to use iterative learning control (ILC) algorithms that have been widely applied in the robotics industry and elsewhere [11, 12, 13, 14, 10, 15, 16]. The learning controller accounts for the unmodeled effects, and is thus suitable in applications where the same maneuver is repeated over and over. This paper expands the simulations in [8] and presents the results of an ILC implementation to achieve specified control objectives based on actual input/output data from the experiments. The experimental implementation of an ILC using a computer-controlled motor-driven vacuum slow wave structure axial displacement mechanism and the resulting performance enhancements are described.

This paper is organized as follows: in section 2 a brief description of learning control is given. Section 3 discusses the experimental set-up and the model of the Sinus-6. In section 4, we discuss the design of ILCs and the two control objectives, and present our simulation and experimental results. Our conclusions and directions for future research are given in section 6.

2 Problem Description and ILC Approach

The problem studied in this paper is the design of a feedback system that can automatically adjust the inputs to the Sinus-6 driven BWO in order to achieve frequency agility or to regulate the power and frequency of the radiated energy at desired set points.

2.1 Learning Control

Modern control theory has been successfully employed in controlling many industrial processes. There are currently many analytical methods to choose a controller that achieves asymptotic stability and an acceptable steady-state error, but few for specifying the transient response of systems (see [17] for example). These limitations motivated researchers to develop new control concepts for systems that repeat the same maneuvers, known as iterative learning control or ILC. Iterative Learning Control deals with processes where the same task that lasts a finite time interval $[0, T]$, is repeated over and over. The objective of the controller is thus to improve the performance with each trial. The concept of iterative learning control was first introduced by Arimoto [11] who proposed a new control concept called betterment process. In that paper, Arimoto suggested a new controller that adds a correcting term to the existing control input after each trial. Since then similar algorithms for different classes of nonlinear systems have been developed [12, 18, 19, 20]. A survey of recent developments in the subject can be found in [10, 15].

The basic idea behind designing an iterative learning controller is generically described in [15] as follows. Consider a nonlinear system described by an operator $f : \mathcal{U} \rightarrow \mathcal{Y}$, where both \mathcal{U} and \mathcal{Y} are normed vector spaces [21]. The control objective is to drive the output $y(t) = f(u(t), t)$ to a desired function $y_d(t)$. This should be achieved by choosing the appropriate input $u^*(t)$ such that a norm $\|y_d(t) - f(u^*(t), t)\|$ is minimized. If the system $f(\cdot)$ is left-invertible, one may choose $u^*(t) = f^{-1}(y_d(t), t)$. In the following, we use $f(\cdot)$ to denote a system which when evaluated at a particular u gives $f(u)$. In most cases, $f(\cdot)$ may not be exactly known and calculating the inverse system may be difficult, if not impossible. In such cases, we would like to find a sequence of inputs

$$u_{k+1}(t) = g(u_k(t), y_k(t), y_d(t), t) \quad (1)$$

such that $u_k(t)$ converges to $u^*(t)$ as the iteration number k goes to infinity. Moreover, we would like to do so without the explicit knowledge of $f(\cdot)$, if possible. This is then the essence of iterative learning control. It turns out in our particular problem, that the BWO model is static and time-invariant so that $y = f(u)$.

A contraction mapping theorem, which is the basis of the ILCs described presented in this paper, may be found in [10, 15].

A block diagram of a learning control scheme is described in Figure 1. The signal y_d is the desired output which we try to make the actual output y track. The error is defined as the difference $y_d - y$. Note that in the figure the controller actually contains two parts, one that is based on the known model and is thus fixed and produces u_m , and another denoted by u_k and obtained as the output of the learning controller. In our simulations, the known model is obtained from the identification we performed in [7], that is the neural network fitted to the actual experimental data.

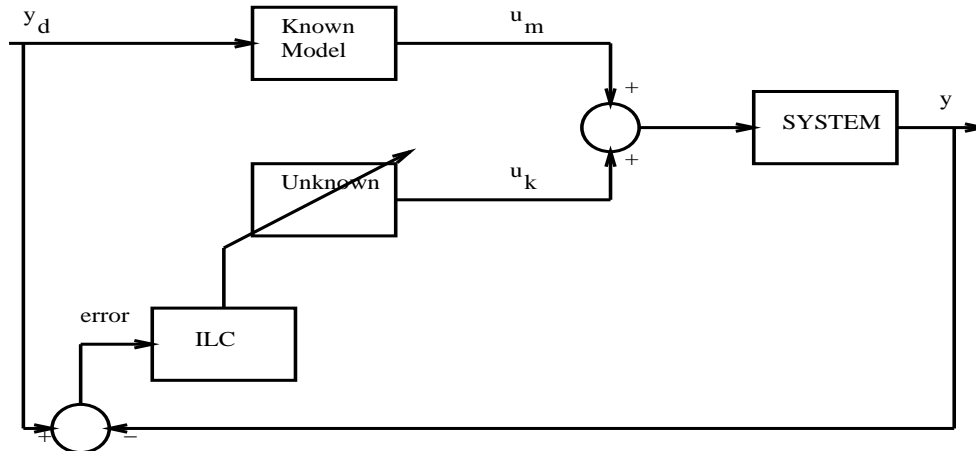


Figure 1: Learning Control Scheme

In the following section, we review our experimental set-up, and present the static model of the BWO to that we apply the learning control ideas described above.

3 Experimental Set-Up

Initial experimentation with the Sinus-6-driven BWO has been reported elsewhere [5, 6], and has yielded input/output data which was used to obtain the model used in this research. We refer next to the block diagram in Figure 2. The block labeled *System S* is identified as the mathematical model in our experiment. The model of the high power BWO consists of an A-K gap (electron gun) delivering an intense electron beam current I that is guided through a slow wave structure by a strong axial magnetic field. There are actually two inputs into this system: the cathode potential $u_1 = V$ and the current $u_2 = I$, while the two measured outputs are the microwave power $y_1 = P$ and the microwave frequency $y_2 = F$. The microwave conversion efficiency $z_1 = E$ is obtained by dividing the peak output microwave power by the input beam power $V \times I$. The voltage V may be adjusted by changing the spark gap pressure, while the current I may be changed by adjusting the A-K gap. In the present research, the A-K gap remains constant, thus fixing the input impedance Z . This translates into a control algorithm whose only output is the voltage V since I is dependent on V through $I = V/Z$. Another control parameter that allows us to achieve frequency agility is the axial displacement of the slow wave structure with respect to the “cutoff neck” inlet to the electromagnetic system [6]. This is what we term “shifting” in this paper.

In this paper we propose and implement two control algorithms: the first regulates the output power and frequency to desired set values, and the other achieves frequency agility by allowing the frequency to change around a center value while maintaining a constant output power. In order to achieve these objectives, the ILC takes the outputs from the BWO and calculates the desired voltage applied to the system to regulate the power and frequency, adjust the output frequency, or to maximize the efficiency. The frequency agility controller is simulated and then implemented in hardware while the regulator is only simulated.

As discussed above, and from the research described in [5], we have access to a set of input cathode voltage

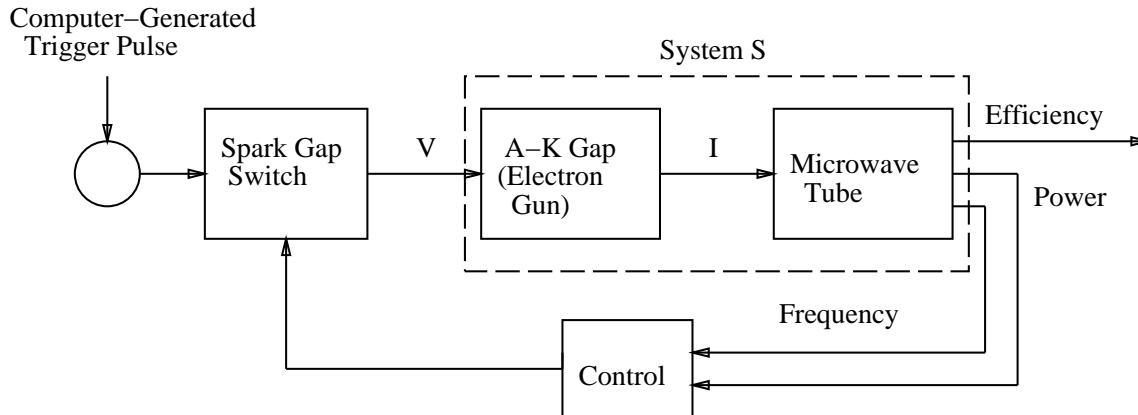


Figure 2: Block-diagram of system.

V , current I and of output microwave efficiency E , power P and frequency F . Due to the complexity of obtaining a physics-based model of high power BWOs, researchers utilize fully electromagnetic particle-in-cell (PIC) codes like MAGIC [22] in order to simulate the operation of these devices. In order to obtain a model suitable for applying our control algorithms, we choose instead to build a model based on the input/output data with the physics providing guidance. We have thus obtained the following static, nonlinear but affine model for the Sinus-6 driven BWO,

$$y = Au + B, \quad u_{min} \leq u \leq u_{max} \quad (2)$$

where $A \in \mathbb{R}^{2 \times 2}$ and $B \in \mathbb{R}^{2 \times 1}$. More specifically we consider

$$\begin{bmatrix} y_1 \\ y_2 \end{bmatrix} = \begin{bmatrix} a_{11} & a_{12} \\ a_{21} & a_{22} \end{bmatrix} \begin{bmatrix} u_1 \\ u_2 \end{bmatrix} + \begin{bmatrix} b_1 \\ b_2 \end{bmatrix} \quad (3)$$

$$z_1 = g(u_1, u_2, y_1, y_2)$$

This model was motivated by the fact that the affine model can simplify the control system design.

The experimental data was collected in four separate experiments, where the A-K gap was adjusted to four different values (the A-K gap determines the electron beam diode impedance). We shall denote these four experimental phase as E_1, E_2, E_3 , and E_4 . The four intervals were divided into 95 sampling points for the first experiment, 102 sampling point for the second experiment, 78 sampling points for the third experiment, and 43 sampling points for the fourth experiment. The experimental data consists of the cathode voltage input $u_1 = V$, the current $u_2 = I$, and the two outputs: total peak power y_1 , frequency y_2 . The RF generation efficiency z_1 was calculated from the formula:

$$z_1 = \frac{P}{V \times I} = \frac{y_1}{u_1 \times u_2}. \quad (4)$$

It turns out that, for the case that output are frequency and total power, four affine neural networks can be used to approximate four experiment phases E_1, E_2, E_3 , and E_4 . But for the case that output is the efficiency, it cannot. This is obvious, because, from equation (4), we see that RF efficiency is not a linear function of the voltage. Instead, we obtain a bilinear fit of the efficiency by taking the ratio of P by the product $V \times I$, where I itself is fitted linearly as a function of V . The affine neural network model was used to fit the experimental input/output data. The objective of the fit is to minimize the following performance objective

$$J = \frac{1}{N} \sum_{i=1}^N [F(W) - y]^2$$

$v's$	I^*	V^*	F^*	P^*	E^*
$0 \leq v_2 \leq 310^{-8}$	6	700	9.936	540.398	0.129
$v_2 = 410^{-8}$	6	532	9.883	495.112	0.155
$v_2 = 510^{-8}$	6	426	9.85	466.539	0.182
$610^{-8} \leq v_2 \leq 10^{-6}$	6	375	9.834	452.791	0.201
$v_2 = 210^{-6}$	3.50	375	9.688	291.373	0.222
$310^{-6} \leq v_2 \leq 1$	2.75	375	9.645	242.948	0.236

Table 1: Results of QEPCAD for experiment E_1

where,

$$W = [a_{11} \ a_{12} \ a_{21} \ a_{22} \ b_1 \ b_2]^T \quad (5)$$

by a choice of the weights W . In general, this is accomplished by a gradient descent procedure of updating the weights as described for example in [23]. In this research, we have used the *backpropagation* training algorithm implemented in the *Neural Network* toolbox of MATLAB. The learned parameters are given in [7] and will be used in the next section to simulate the controllers.

4 Design of Iterative Learning Controllers

The design of ILCs consists of choosing the mapping $g(\cdot)$ in (1) so that it is a contraction mapping as described in [10]. The idea of using a contraction mapping is useful in trying to show the in many algorithms since once a mapping is shown to contract distances, and using the fact that vectors getting close to each other must be getting close to a unique vector, convergence of the iteration algorithm is guaranteed. For our case, the system to be controlled is given as in equation (2) by $y = Au + B$. Note again that because our system is static, no time dependence appears. The ILC structure used is of the form

$$\begin{aligned} u_{k+1} &= u_k + p(e_k) \\ e_k &= y_d - y_k \end{aligned} \quad (6)$$

where $y_k = Au_k + B$, k is the iteration number, and p is an operator (static or dynamic) to be designed such that the conditions of the contraction mapping are satisfied [10, 15]. In the following, we show how to choose p for two different control objectives.

4.1 Controlling Radiated Power and Frequency

Next, we discuss an approach for obtaining voltage and current set points that will maximize the output power along with the RF conversion efficiency. In order to solve the set point design problem, we resort to the use of quantifier elimination (QE) methods. We used a software package called QEPCAD [24] in order to implement such algorithms. QEPCAD software produced the results in Table 1 for experiment E_1 , and for different v_1, v_2 combinations. A more detailed description of this approach may be found in [25]. We can see that with I decreasing and V decreasing, the power P is decreased but the efficiency E is increased. Now that we have the desired set points, we proceed to implement the ILC to regulate V and I . In what follows, we use the following ILC,

$$u_{k+1}(t) = u_k(t) + p(t) * e_k(t)$$

where the symbol $*$ denotes convolution and the filter whose impulse response is $p(t)$ is chosen to satisfy the norm inequality

$$\|I - P(jw)A\|_{\infty} = \sup_w \bar{\sigma}(I - P(jw)A) < 1, \quad \forall w \in R \quad (7)$$

where $\bar{\sigma}$ denotes the largest singular value and \sup denotes the supremum. This then insures that the conditions of the contraction mapping theorem hold. We choose $I - P(j\omega)A = H(j\omega)$, where $H(j\omega) \in \mathcal{R}^{2 \times 2}$ satisfies inequality (7), and \mathcal{R} is the set of rational transfer functions. For our purpose, we have chosen $H(j\omega)$ diagonal with entries having norm less than one. Then $P(j\omega)$ can be computed as follows

$$\begin{aligned} P(j\omega)A &= H(j\omega) + I \\ P(j\omega)A &= \begin{bmatrix} H_{11}(j\omega) + 1 & 0 \\ 0 & H_{22}(j\omega) + 1 \end{bmatrix} \end{aligned} \quad (8)$$

where $\|H_{11}(j\omega)\|_\infty$ and $\|H_{22}(j\omega)\|_\infty$ are less than 1. For simulation purposes, we choose

$$H_{11}(j\omega) = H_{22}(j\omega) = \frac{K}{s + \alpha}, \quad \alpha > 0, \quad |K/\alpha| < 1$$

In order to illustrate our ILC performance, we choose a nominal model in our simulation as obtained from [7]

$$A_m = \begin{bmatrix} 0.0016 & -0.0533 \\ 1.1428 & -13.533 \end{bmatrix}, \quad B_m = \begin{bmatrix} 9.0741 \\ -237.37 \end{bmatrix} \quad (9)$$

and assume that the actual plant is given by

$$A = \begin{bmatrix} 0.0004 & 0.0627 \\ 0.5331 & 72.379 \end{bmatrix}, \quad B = \begin{bmatrix} 9.2798 \\ -246.25 \end{bmatrix} \quad (10)$$

The desired output response was $F_d = 9.834$ GHz and $P_d = 452.791$ MW. We thus use the structure in Figure 1 to design an ILC controller with a nominal component obtained from the nominal model, and a learning controller designed based on the ILC concepts. The simulation results are shown in Figure 3. Note that both frequency and peak power are regulated to their desired values after a couple of iterations, and that the current and voltage inputs stabilize to their desired values. Note that in practice this takes a very short time, allowing time for the mechanical adjustment between successive firings of the accelerator to achieve the results.

4.2 Frequency Agility

In this case, our control objective is to keep a constant output power when we axially displace the slow wave structure, and thus change the output frequency [6]. Note that in the previous section, the main concern was to control both output variables, namely the frequency and power, by adjusting the input current and voltage, with no constraints on the inputs. In practice this is possible if the control variables are independent. However, as mentioned earlier, our only accessible variable is the pressure (or voltage) and the input current is a linear function of this voltage.

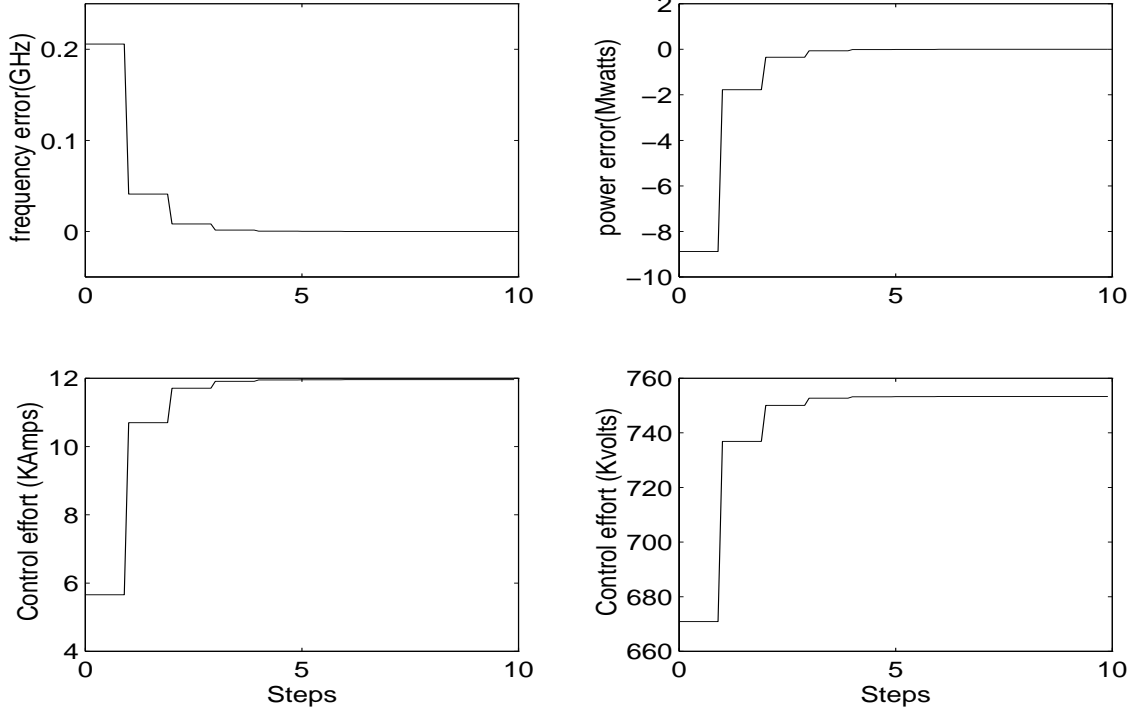
$$V = I \times Z \quad (11)$$

The frequency-agility control problem can thus be reformulated as follows: given a desired output power, find the control signal to drive the error between the measured output power and the desired one to zero, with the constraint $\frac{V_k}{I_k} = Z = \text{constant}$, where k denotes the iteration number. Now that the only output variable to be controlled is the power, we have

$$\begin{aligned} P_k &= a_{11}V_k + a_{12}I_k + b_1 \\ &= \left(a_{11} + \frac{a_{12}}{Z}\right)V_k + b_1 \end{aligned} \quad (12)$$

where the pair (a_{11}, a_{12}) is the first row of the matrix A , V_k and I_k are the control efforts at the k -th trial, and P_k the corresponding output measured power. Now define $\alpha = \left(a_{11} + \frac{a_{12}}{Z}\right)$ and $u_k = V_k$. The control effort is of the form

$$u_k = u_{k-1} + \Gamma e(k-1) \quad (13)$$

Figure 3: Plot of the output error and control effort response for $\alpha = 5$, $K = 1$

where $\Gamma \in \mathbb{R}$ is the vector gain to be calculated and $e(k) = P_d - P_k$, where P_d is the desired output power. The actual output power can then be written in the form

$$\begin{aligned} P_k &= \alpha u_k + b_1 \\ &= \alpha(u_{k-1} + \Gamma e_{k-1}) + b_1 \\ P_k &= P_{k-1} + \alpha \Gamma e_{k-1} \end{aligned}$$

or finally,

$$\begin{aligned} P_d - P_k &= P_d - P_{k-1} - \alpha \Gamma e_{k-1} \\ e_k &= [1 - (\alpha \Gamma)] e_{k-1} \end{aligned} \quad (14)$$

From equation (14), it is easy to see that in order to satisfy the conditions of contraction mappings [10], we need to choose Γ such that $0 < \alpha \Gamma < 1$. We have chosen in our simulations the value $\alpha \Gamma = 0.8$, and $\frac{V_k}{I_k} = 135$ Ohms. Note that in reality, and since Γ is not exactly known, we may need to design an adaptive gain α in order to guarantee that $\alpha \Gamma < 1$. This will be a topic of future research. The simulation was performed for four different shifts of the slow wave structure (SWS), and the plots in Figure 4 show that for every shift in the SWS, the control efforts are automatically adjusted, keeping the impedance value constant. In fact, notice that the difference between the desired peak power output and the actual output goes to zero after each shift and after 1 shot. The frequency of the output is allowed to vary between 9.3 GHz and 9.65 GHz, while the voltage input (and thus the current) is adjusted to counteract the effect of shifting on radiated power [6].

5 Control Implementation on the Sinus-6

Figure 5 is a block diagram of the LabView program written for data acquisition and control purposes. The output variables are frequency (GHz) and power (MW).

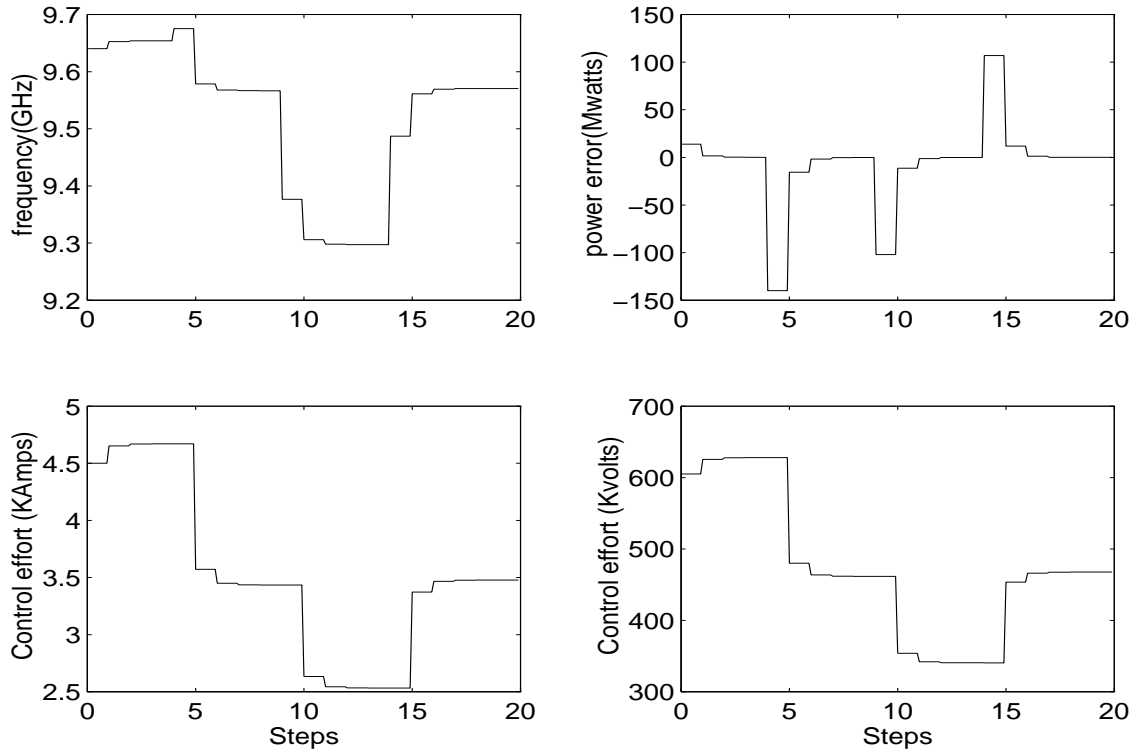


Figure 4: The Frequency Agile ILC Performance

The frequency of the radiated microwave is a sinusoidal function of the displacement of the SWS with respect to the cutoff neck. Experimental results, for a fixed cathode voltage, have shown that the period of the sinusoidal variations in frequency is about 16 mm. These variations provide a frequency bandwidth of 300 MHz, ranging between 9.45 GHz and 9.75 GHz. The lateral shifting of the SWS is achieved using a vacuum compatible BWO step motor mechanism that is controlled by LabView through the serial port using an RS-232 connection. Figure 6 shows the experimental results for the frequency versus forward shifting of the SWS. Note, however that the frequency of the microwave is also a function of the cathode voltage, and

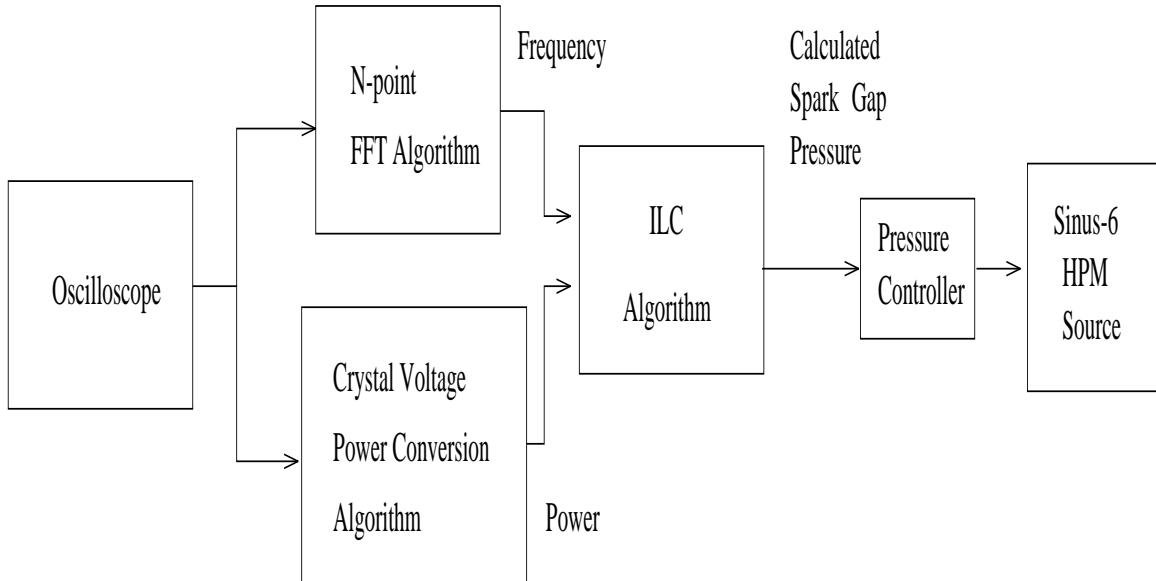


Figure 5: Block diagram of the LabView program for measurement and control purposes.

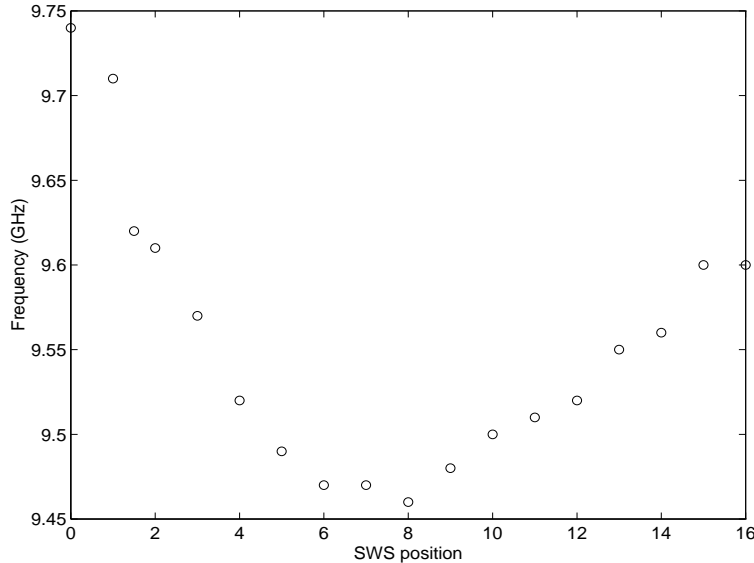


Figure 6: Experimental results of frequency vs SWS position.

for higher voltages this frequency curve is just shifted in the frequency-axis.

5.1 Pressure Controller

The cathode voltage is controlled by changing the spark gap pressure. The ILC algorithm calculates the desired spark gap voltage after each shot by trying to adjust for the power error signal. A block diagram for the pressure control system is given in Figure 7.

The input to the spark gap from the nitrogen tank is a constant step input of 2000 psi. The flow of nitrogen gas into the spark gap is controlled by on-off electromechanical pressure valves. The easiest way to control the pressure inside the spark gap is to introduce on-off nonlinearities, but such controllers are known to cause limit cycle oscillations in the output if not properly designed. One way to eliminate limit cycles is to analyze the behavior of the closed loop system using describing functions to characterize the nonlinearities in our controller [21]. Suppose that the input to the nonlinear element is sinusoidal, and assume that the output is another waveform of the same period, but with higher harmonics. In the describing-function analysis it is assumed that only the fundamental component of the output is significant. Such an assumption is valid since the higher harmonics in the output of a nonlinear element are often of smaller amplitude than the amplitude of the fundamental harmonic component. In addition, most control systems are low-pass filters, with the result that the higher components are very much attenuated compared with the fundamental component. The describing function is defined to be the complex ratio of the fundamental component of the output to the input. This assumption works well when the amplitude of the higher harmonics are small enough not to change the output of the nonlinear element.

For our design, we considered three different pressure controllers. The on-off nonlinear controller was the easiest to realize, but was highly sensitive to noise, and when the error signal was different from zero, eliminating high-frequency oscillations turned out to be impossible. Another option was to introduce saturation nonlinearity. In this case, for small error signals, the output is proportional to the input error signal, and for larger input error signals, the output control effort is constant at the maximum possible output value. However, in order to activate the actuators, this design required a high proportional gain to amplify small error signals, which in turn amplified noise and higher harmonic components and again eliminating oscillations in the output was impossible. The third type of pressure controller introduced an on-off nonlinearity with dead-zone and hysteresis (see Figure 7). The dead zone is around 20 mV, and the hysteresis is 10 mV. The

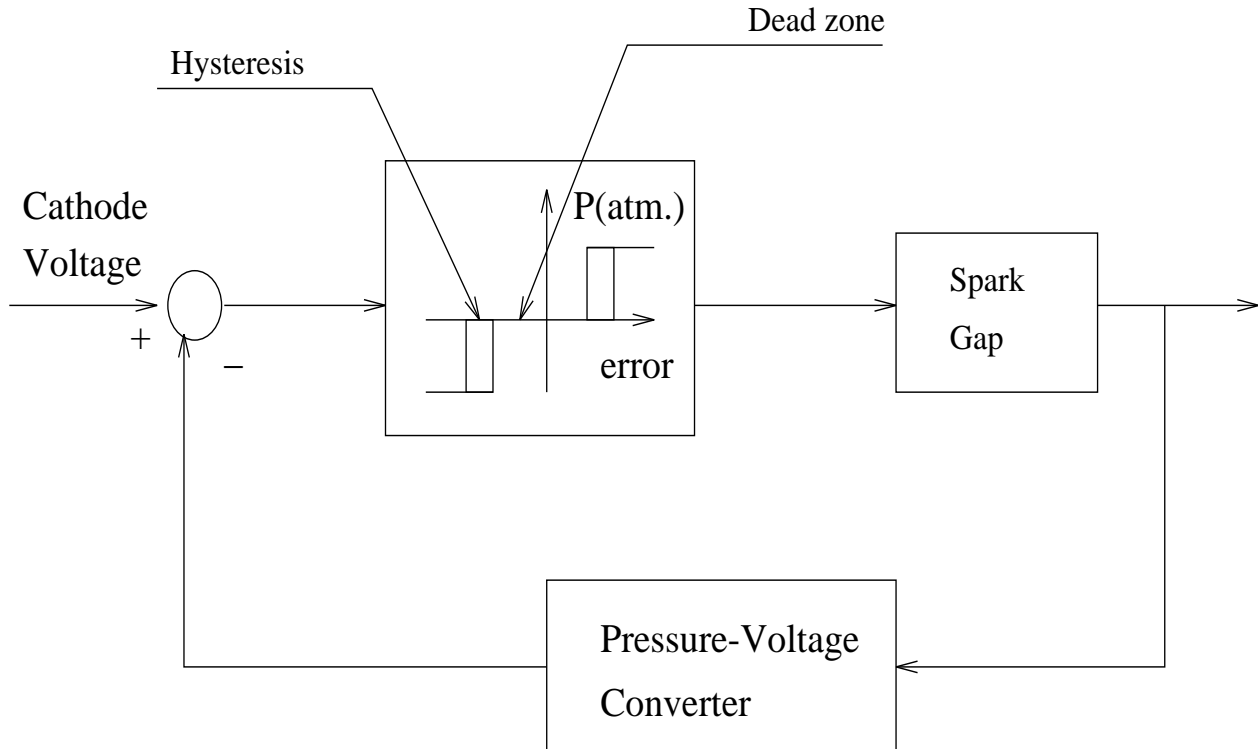


Figure 7: Block diagram of the pressure control system.

dead zone eliminates high frequency oscillations of very small amplitude when the error signal between the desired cathode voltage and the spark gap self-breakdown voltage is close to zero. The hysteresis prevents further oscillations in the output due to the presence of noise, providing enough gap before triggering the actuators. To realize this controller an analog electronic circuit was built. Figure 8 shows the circuit diagram for the pressure controller.

In order to find a relationship between the input to the controller and the desired cathode voltage, a first-order curve fit was obtained based on measurements performed at different pressure values. Table 2 shows the reference input voltage to the controller for different cathode voltages. The first order-fit line was of the form $V_{ref} = 0.0055V_{cathode} - 0.6985$.

Table 2: Experimental results on spark gap pressure and the corresponding cathode voltage.

Pressure (atm)	Cathode Voltage (KV)	Reference input (V)
9	483	1.96
9.5	507	2.166
10	531	2.286
10.5	566	2.407
11	592	2.53
12	650	2.77
13	664	3.023
13.5	688	3.15
14	704	3.27
14.5	725	3.42
15	740	3.51

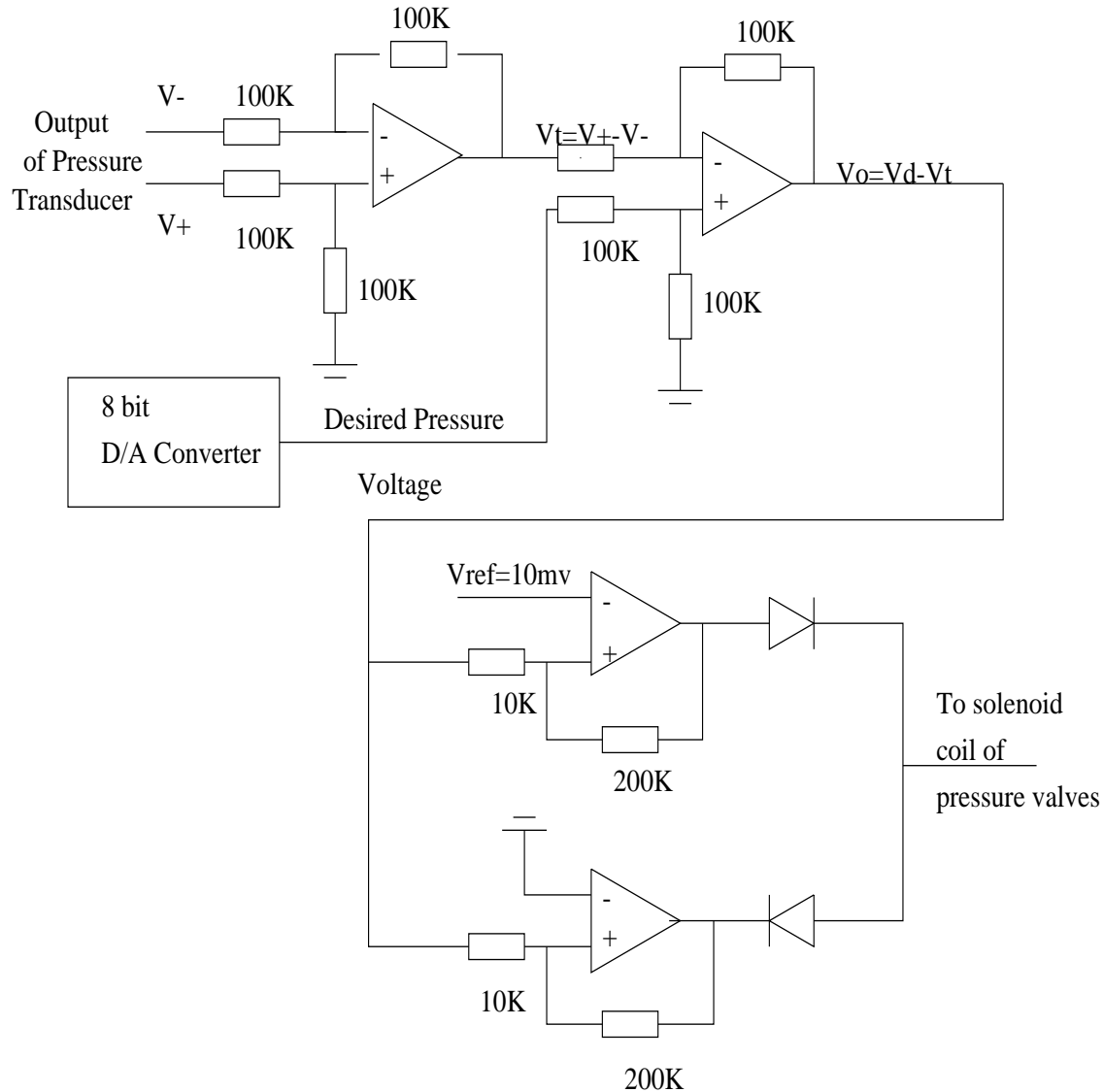


Figure 8: Circuit diagram of the pressure control system.

5.2 Iterative Learning Controller Design

As mentioned earlier, the objective of our experiment is to design a controller that maintains a constant power over a frequency range of 300MHz. In order to do so, it is desirable to have an approximate model of the plant. However, the complexity of the behavior of our system at different voltages and SWS displacements requires the knowledge of the different models of the plant at every shift of the SWS. In other words, the output microwave power can be represented as a function of two variables: $P_{out} = f(V_{cathode}, d_{SWS})$, where $480\text{KV} \leq V_{cathode} \leq 750\text{KV}$ and $0 \leq d_{SWS} \leq 8\text{mm}$.

Data indicates that the maximum output power can be achieved when $d_{SWS} = 0\text{mm}$, and the minimum at $d_{SWS} = 8\text{mm}$. Measurements of power as a function of cathode voltage were obtained at the maximum possible output power, and it turned out that, at a fixed displacement of the SWS, the power was a strictly monotonic function of the cathode voltage. Table 3 shows average power values at different cathode voltages.

Figure 9 is a plot of power versus cathode voltage at a fixed position of the SWS. A first order fit was obtained for this set of data points, where $P(V) = 0.68V - 265.75$. It is obvious that power is a continuous function of the cathode voltage and is strictly monotonic. For different positions of the SWS it is also obvious

Table 3: Experimental results on microwave output power at different cathode voltages and the corresponding first-order fit.

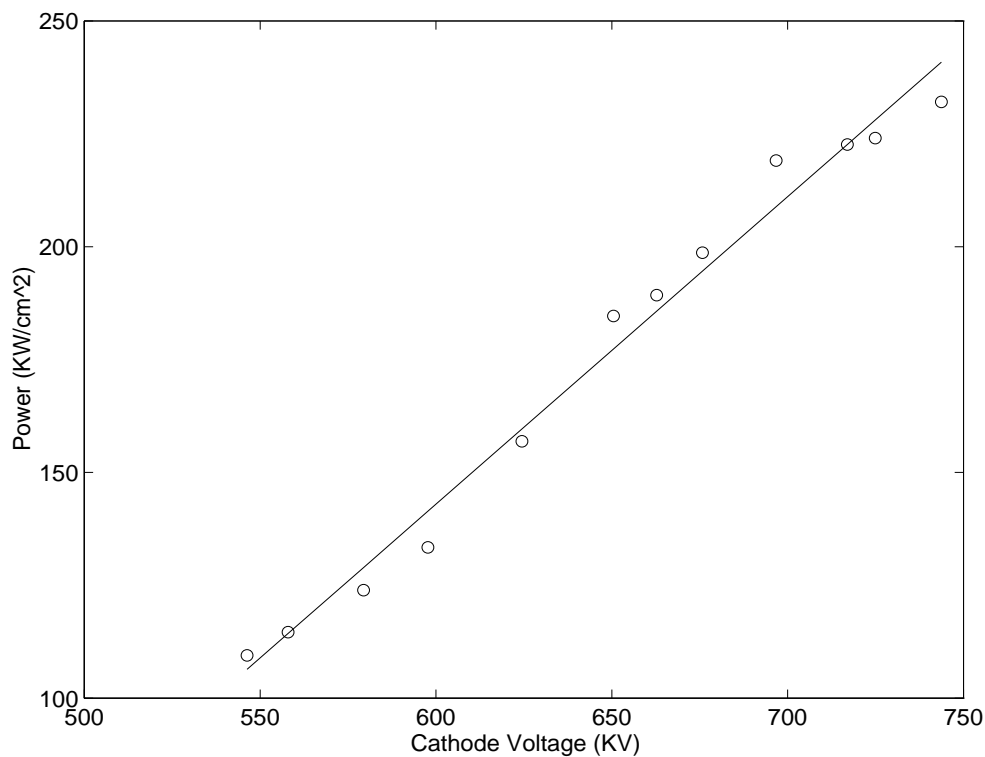
Cathode Voltage (KV)	Output Power (KW/cm ²)
546	109
557	114
579	123
597	133
624	156
650	184
662	189
675	198
696	219
716	222
724	224
743	232

that this curve will simply shift downwards. Now, since our function is monotonic and continuous it satisfies a Lipschitz condition, i.e $\exists L > 0$ such that

$$|P(V_2) - P(V_1)| \leq L|V_2 - V_1|. \quad (15)$$

For our design purpose the iterative learning control algorithm was chosen to be of the form, according to the designs in section 4.2,

$$V_k = V_{k-1} + \Gamma(P_d - P(V_{k-1})). \quad (16)$$

Figure 9: Power density (KW/cm²) versus cathode voltage for d=0mm.

The error equation in this case becomes

$$|e_k| \leq |1 - L\Gamma||e_{k-1}|, \quad (17)$$

where P_d is the desired output microwave power and $P(V_{k-1})$ is the output power after $k - 1$ shots. For the ILC algorithm to converge it is sufficient to have $|1 - L\Gamma| < 1$, whereas the condition derived in section 4.2 was necessary and sufficient. Initially $\Gamma = 0.5$ was chosen, however the number of iterations was large so that after trial and error, a value of $\Gamma = 2$ was chosen; The learning controller was tested for five different shifts of the SWS, with $d=8$ mm, 6 mm, 4 mm, 2 mm, 0 mm, and the desired output microwave power density was $95KW/cm^2$. Figures 10 - 14 show the control effort, frequency, and output microwave power and the number of iterations required for convergence to within an error of five percent.

In Figure 10, the SWS displacement was set to 0 mm with respect to the cut-off neck, and the desired output power of the microwave source was set at $95 KW/cm^2$; however, the frequency was allowed to vary within a range of 300 MHz. We began the experiments with an arbitrary initial condition on the cathode voltage. For the next four iterations it is obvious that the ILC is trying to adjust the cathode voltage based on the error in the output power. Note that during the fourth iteration, the cathode voltage is slightly higher than the estimated one, a phenomenon due to the jitter in the self breakdown voltage of the spark gap as a function of pressure. However, this can be corrected for by accounting for such irregularities. In fact, the ILC was able to correct for this error after two more iterations, resulting in the output power converging to the desired value. Note that at this voltage and SWS position the frequency of the microwave signal was 9.45 GHz.

In Figure 11, the SWS position was set to 2 mm, keeping the desired power constant, and we repeated the same experiment taking into consideration any inconsistencies in the self breakdown voltage of the spark gap. The ILC in this case showed that after three iterations the output power has converged to within 5 percent of the desired power. Here again the frequency was allowed to vary between 9.53 and 9.56 GHz, with a final value of around 9.535 GHz.

In Figure 12, the SWS position was set to 4mm, and again three iterations were sufficient to converge to the desired power value with a frequency range between 9.45 and 9.5 GHz, and a final value of around 9.5 GHz. Here the ILC showed that three iterations were sufficient for convergence, since the initial cathode voltage was close enough to the desired voltage.

Similar results are shown in Figures 13 and 14.

In Figure 15 we have included all experimental results obtained for the five different positions of the SWS, between 8mm and 0mm. Notice how the ILC adjusts the cathode voltage after shifting of the SWS trying to maintain the output power at a constant level. In this particular example we were able to achieve frequency agility of the BWO, with the frequency varying between 9.4 and 9.6 GHz.

6 Conclusions and Future Work

In this paper, we have presented an iterative learning controller approach in trying to design smart microwave tubes. This control structure was chosen because of its ability to improve its performance in systems such as the repetitively-pulsed Sinus-6 BWO. Our control design was built around our previous experience in modeling the Sinus-6 BWO, our earlier research on frequency agility, and on our control system experience. The controller we designed, simulated, and implemented was shown to be effective in regulating the output frequency and peak power output, and in achieving frequency agility.

The iterative learning controller was tested on the high power microwave source, to maintain constant output power for a given range of frequencies. Experimental results were also included to show the effectiveness of this simple but robust controller. Note that we have required little knowledge of the plant model, except that it satisfy a Lipschitz condition over the range of operation. The controller was successful in learning the behavior of the microwave source at every shot, trying to minimize the error signal between the output power and a desired output level. This paper thus illustrated in hardware the viability of automating

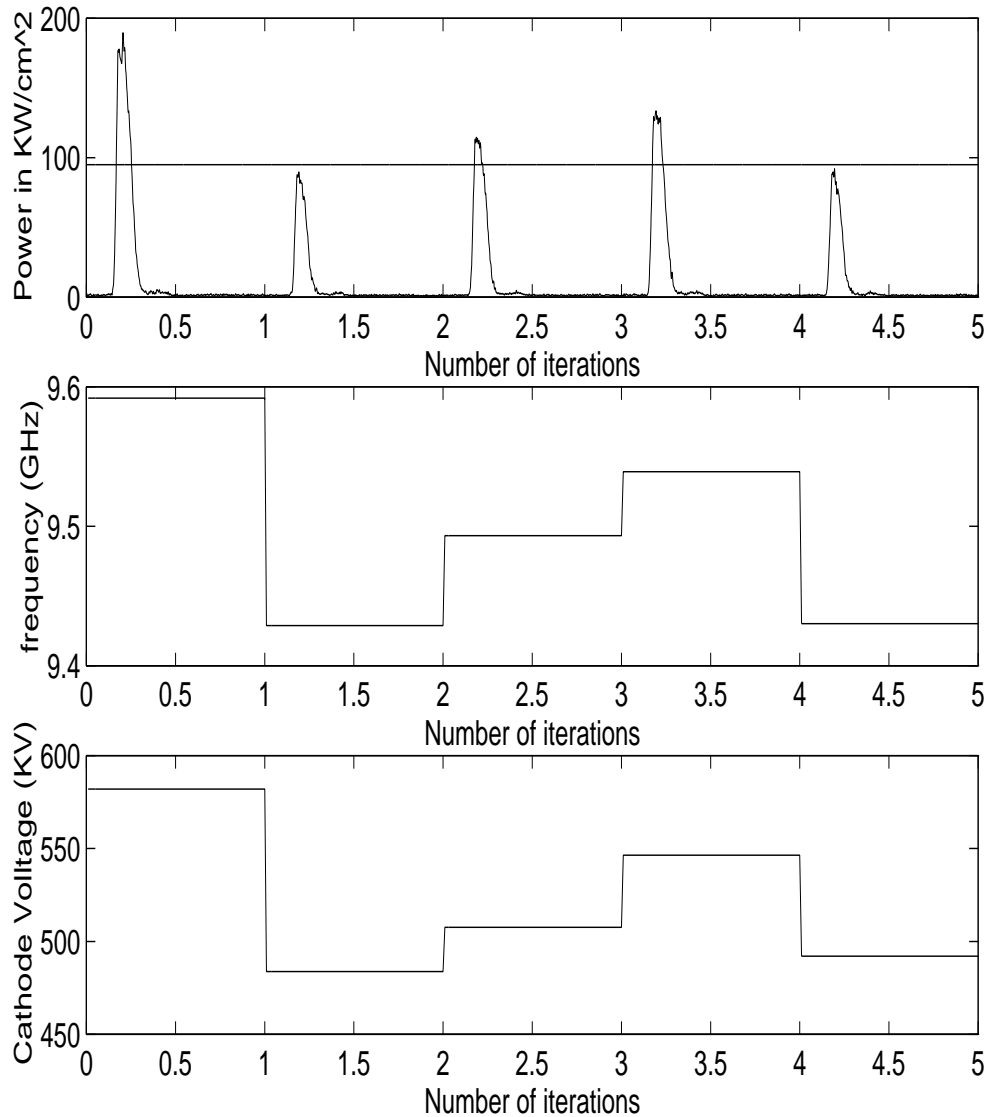


Figure 10: Performance of ILC for $P_d = 95 \text{ KW}/\text{cm}^2$ and $d = 0 \text{ mm}$.

the operation of a frequency agile BWO. So far we were successful in maintaining constant output power while frequency was allowed to change. Future research can extend the results obtained here to control the frequency as well. Our limitations were due to the fact that we were able to use only one control input signal, the cathode voltage, to control the power, while neglecting the dependency of frequency on both slow wave structure (SWS) position and power. A second control input, the SWS position in this case, can be utilized to maintain a desired output frequency. We were able to show that output power can be maintained constant independent of SWS position. This independence allows us to design a separate controller for changing the SWS position, while maintaining a constant power. Experimental results have shown that frequency is a sinusoidal function of SWS displacement. This enables us to implement a similar iterative algorithm to find the desired SWS position, while maintaining power constant at each iteration that achieves the desired frequency. The advantage of this proposed method is that the two controllers can be designed dependently, and stability issues can be dealt with separately. Its main disadvantage however, is that the number of iterations for convergence of both frequency and power increases.

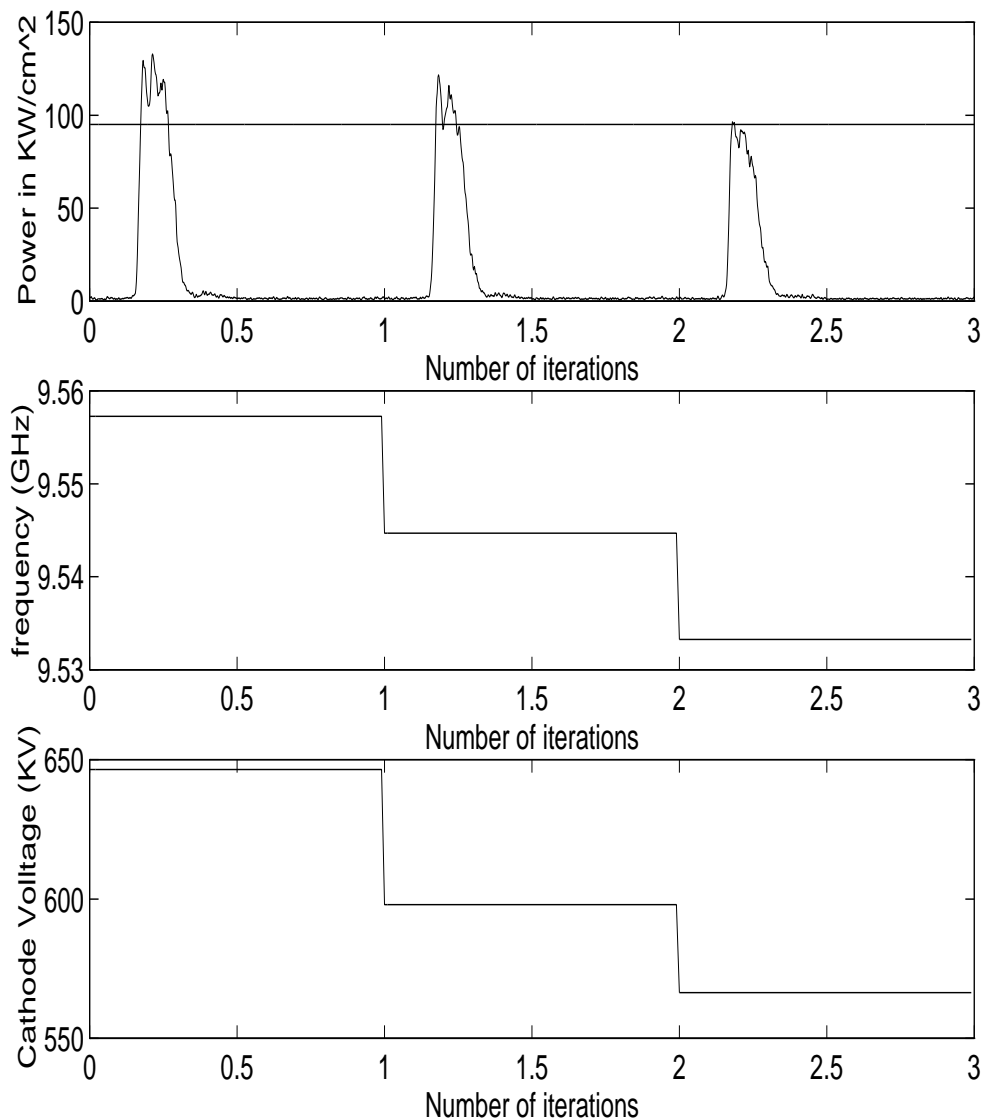


Figure 11: Performance of ILC for $P_d = 95 \text{ KW/cm}^2$ and $d = 2 \text{ mm}$.

References

- [1] J. Benford and J. Swegle, *High Power Microwaves*. Boston, MA: Artech House, 1992.
- [2] C. Taylor and D. Giri, *High-Power Microwave Systems and Effects*. Washington, DC: Taylor & Francis, 1994.
- [3] R. Miller, "Pulse shortening in high-peak-power reltron tubes," *IEEE Trans. Plasma Sci.*, vol. This issue, 1997.
- [4] D. Price, J. levine, and J. Benford, "Diode plasma effects on the microwave pulse length from relativistic magnetrons," *IEEE Trans. Plasma Sci.*, vol. This issue, 1997.
- [5] L. Moreland, E. Schamiloglu, R. Lemke, S. Korovin, V. Rostov, A. Roitman, K. Hendricks, and T. Spencer, "Efficiency enhancement of high power vacuum BWO using nonuniform slow wave structures," *IEEE Trans. Plasma Sci.*, vol. 22, no. 2, pp. 554–565, 1994.

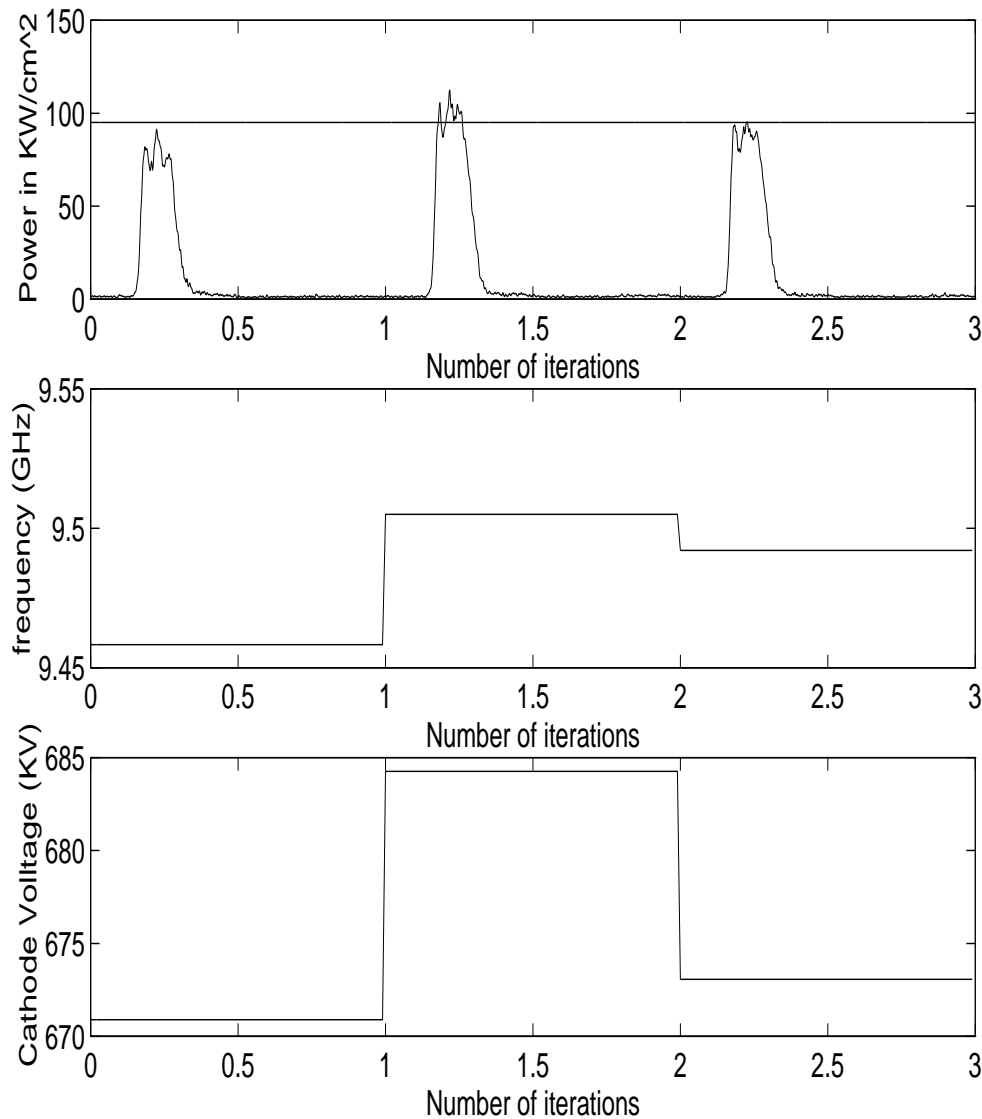


Figure 12: Performance of ILC for $P_d = 95 \text{ KW/cm}^2$ and $d = 4 \text{ mm}$.

- [6] L. Moreland, E. Schamiloglu, R. Lemke, A. Roitman, S. Korovin, and V. Rostov, "Enhanced frequency agility of high power relativistic backward wave oscillators," *IEEE Trans. Plasma Sci.*, vol. 24, no. 2, pp. 852–858, 1996.
- [7] C. Abdallah, W. Yang, E. Schamiloglu, and L. Moreland, "A neural network model of the input/output characteristics of a high power backward-wave oscillator," *IEEE Trans. Plasma Sci.*, vol. 24, no. 3, pp. 879–883, 1996.
- [8] C. Abdallah, V. Soualian, and E. Schamiloglu, "Towards "smart tubes" using iterative learning control," *IEEE Trans. Plasma Sci.*, To appear: 1998.
- [9] R. Smith and A. Packard, "Optimal control of perturbed linear static systems," *IEEE Trans. Automat. Control*, pp. 579–584, 1996.
- [10] K. L. Moore, *Iterative Learning Control For Deterministic Systems*. Berlin–Heidelberg–New York: Springer-Verlag, 1st ed., 1992.

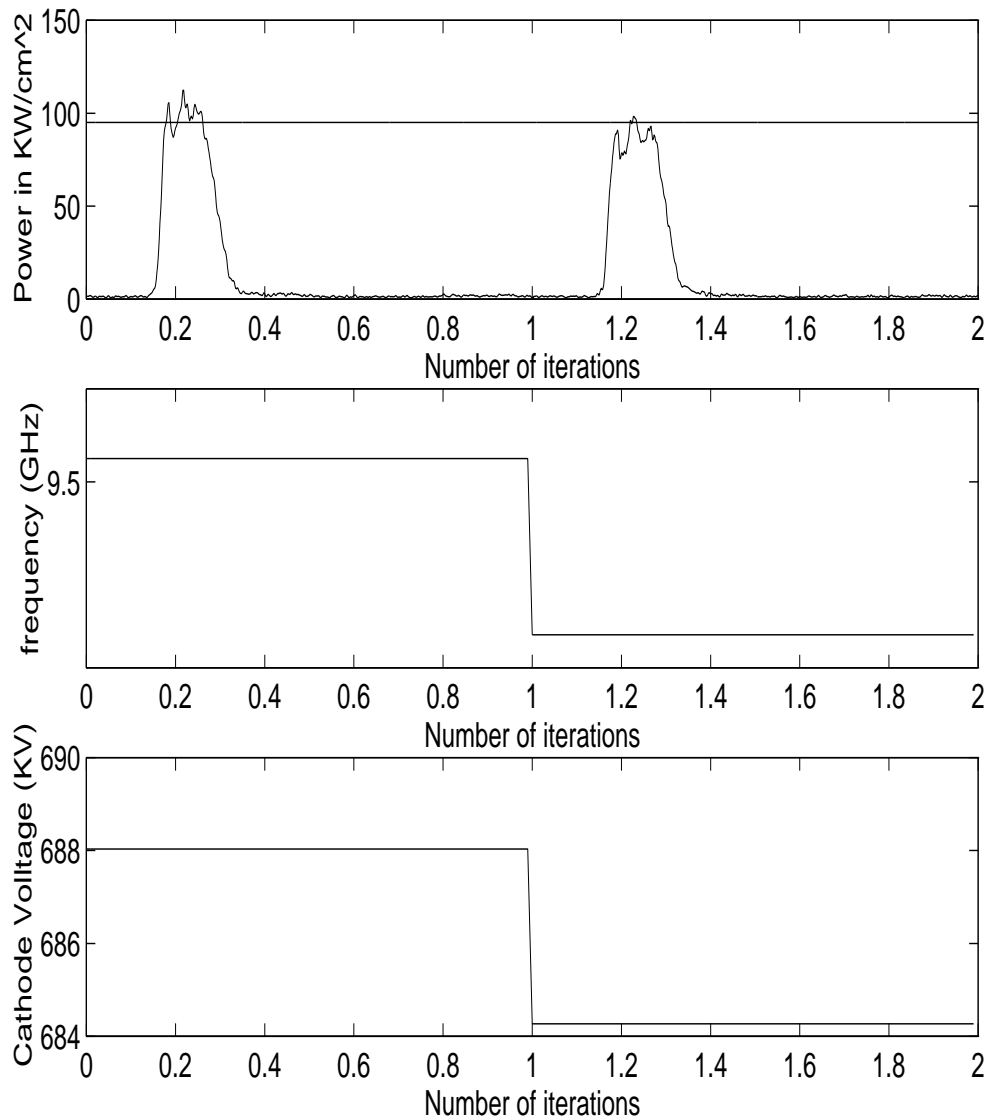


Figure 13: Performance of ILC for $P_d = 95 \text{ KW/cm}^2$ and $d = 6 \text{ mm}$.

- [11] S. Arimoto, S. Kawamura, and F. Miyazaki, "Bettering operation of dynamic systems by learning: A new control theory for servomechanism or mechatronic systems," in *Proceedings of the 23rd Conference on Decision and Control*, vol. 2, pp. 1064–1069, December 1984.
- [12] T. Sugie and T. Ono, "An iterative learning control law for dynamical systems," *Automatica*, vol. 27, no. 4, pp. 729–732, 1991.
- [13] S. Hara, Y. Yamamoto, T. Omata, and M. Nakano, "Repetitive control system: A new type servo system for periodic exogenous signals," *IEEE Transactions on Automatic Control*, vol. 33, pp. 659–667, July 1988.
- [14] J. J. Craig, *Adaptive Control of Mechanical Manipulators*. United States: Addison-Wesley, Inc., 1st ed., 1988.
- [15] K. L. Moore, "Iterative learning control—an expository overview," *Applied and Computational Controls, Signal Processing, and Circuits*, p. To appear, 1997.

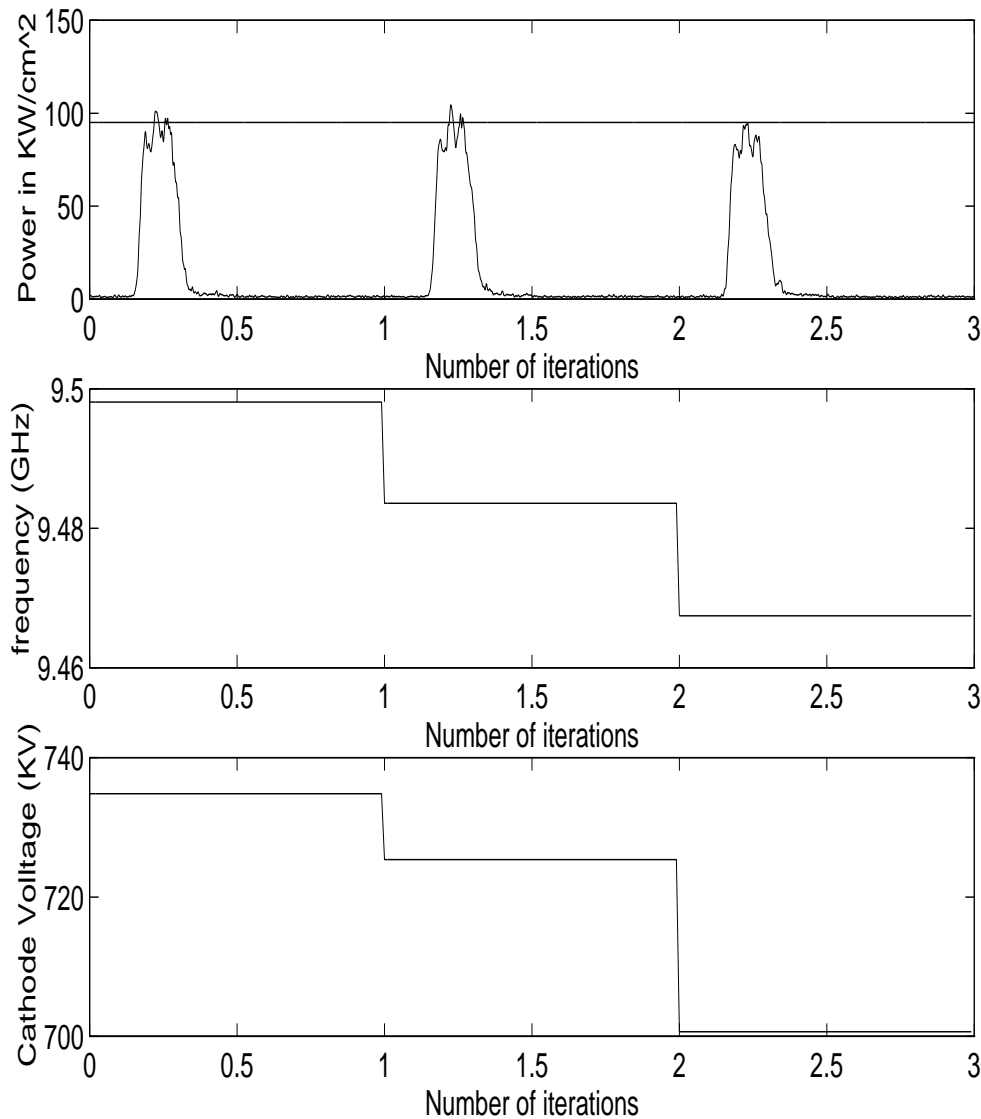


Figure 14: Performance of ILC for $P_d = 95 \text{ KW/cm}^2$ and $d = 8 \text{ mm}$.

- [16] E. Rogers and D. H. Owens, *Stability Analysis for Linear Repetitive Processes*. Berlin–Heidelberg–New York: Springer-Verlag, 1st ed., 1992.
- [17] T. Kailath, *Linear Systems*. Englewood Cliffs, N.J.: Prentice-Hall, Inc., 1st ed., 1980.
- [18] T.-Y. Kuc, J. S. Lee, and K. Nam, “An iterative learning control theory for a class of nonlinear dynamical systems,” *Automatica*, vol. 28, no. 6, pp. 1215–1221, 1992.
- [19] P. Bondi, G. Casalino, and L. Gambardella, “On the iterative learning control theory for robotic manipulators,” *IEEE Journal of Robotics and Automation*, vol. 4, pp. 14–22, February 1988.
- [20] T.-Y. Kuc, K. Nam, and J. S. Lee, “An iterative learning control of robot manipulators,” *IEEE Transactions on Robotics and Automation*, vol. 7, pp. 835–842, December 1991.
- [21] M. Vidyasagar, *Nonlinear Systems Analysis*. Englewood Cliffs, N.J.: Prentice-Hall, Inc., 2nd ed., 1993.
- [22] B. Goplen, L. Ludeking, D. Smithe, and G. Warren, “User-configurable magic for electromagnetic pic calculations,” *Comp. Phys. Comm.*, vol. 87, pp. 54–86, 1995.

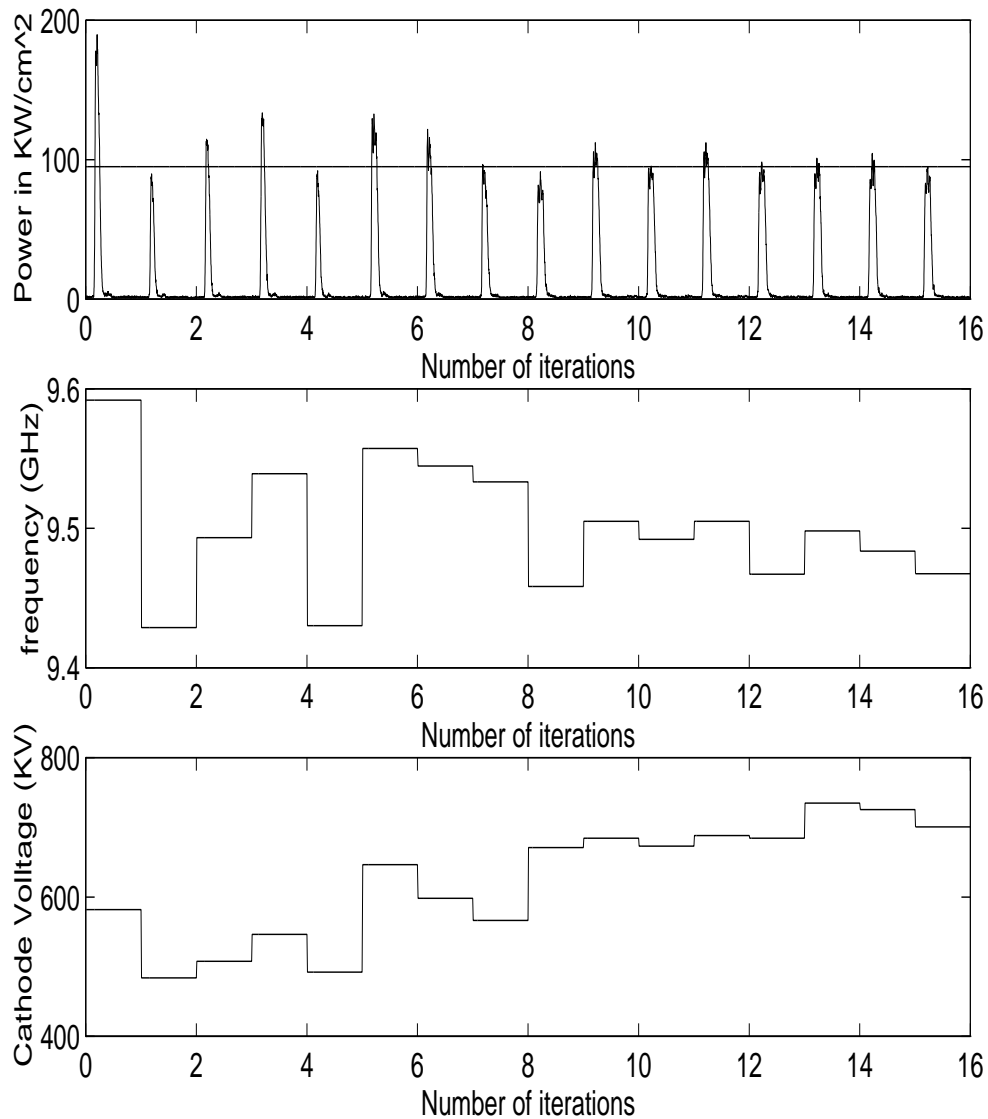


Figure 15: Performance of ILC for $P_d = 95 \text{ KW/cm}^2$ and $d = 0 - 8 \text{ mm}$.

- [23] P. Baldi, "Gradient descent learning algorithm overview: A general dynamical systems perspective," *IEEE Trans. Neural Nets*, vol. 6, no. 1, pp. 182–195, 1995.
- [24] H. Hong, "Parallelization of quantifier elimination on workstation network," Tech. Rep. 91-55.0, Johannes Kepler University, RISC-Linz, 1991.
- [25] C. Abdallah, W. Yang, E. Schamiloglu, and V. Souvalian, "On the control of a high power backward-wave oscillator using quantifier elimination methods," in *Proceedings of the American Control Conference*, pp. 3255–3256, 1997.